Astronomy & Astrophysics

Magnetic flux cancellation associated with a recurring solar jet observed with *Hinode*, *RHESSI*, and *STEREO*/EUVI[⋆]

C. Chifor[1], H. Isobe[2], H. E. Mason[1], I. G. Hannah[3], P. R. Young[4], G. Del Zanna[5], S. Krucker[6], K. Ichimoto[2], Y. Katsukawa[7], and T. Yokoyama[8]

[1] Department of Applied Mathematics and Theoretical Physics, Centre for Mathematical Sciences, Wilberforce Road, Cambridge CB3 0WA, UK
e-mail: c.chifor@damtp.cam.ac.uk
[2] Kwasan and Hida Observatory, Kyoto University, Yamashina, Kyoto 607-8471, Japan
[3] Department of Physics and Astronomy, University of Glasgow, Glasgow, G12 8QQ, UK
[4] STFC Rutherford Appleton Laboratory, Chilton, Didcot, Oxfordshire OX11 0QX, UK
[5] Mullard Space Science Laboratory, University College London, Holmbury St. Mary, Dorking, Surrey RH5 6NT, UK
[6] Space Science Laboratory, University of California at Berkeley, Berkeley, CA 94720-7450, USA
[7] Institute of Space and Astronautical Science, Japan Aerospace Exploration Agency, 3-1-1 Yoshindai, Sagamihara, Kanagawa, 229-8510, Japan
[8] Department of Earth and Planetary Science, University of Tokyo, Hongo, Bunkyo-ku, Tokyo 113-0033, Japan

ABSTRACT

Aims. We study the physical properties of a recurring solar active region jet observed in X-rays and extreme-ultraviolet (EUV).
Methods. Multi-wavelength data from all three instruments on board *Hinode* were analysed. X-ray imaging and spectroscopy of the microflaring emission associated with the jets was performed with the *Reuven Ramaty High Energy Spectroscopic Imager* (*RHESSI*). Associated EUV jets were observed with the Sun Earth Connection Coronal and Heliospheric Investigation (SECCHI)/Extreme Ultraviolet Imager (EUVI) on board *STEREO*.
Results. We found a correlation between recurring magnetic flux cancellation close to a pore, the X-ray jet emission, and associated Ca II H ribbon brightenings. We estimated the lower limit for the decrease in magnetic energy associated with the X-ray jet emission at 3×10^{29} erg. The recurring plasma ejection was observed simultaneously at EUV and X-ray temperatures, associated with type III radio bursts and microflaring activity at the jet footpoint.
Conclusions. The recurring jet (EUV and X-ray) emissions can be attributed to chromospheric evaporation flows due to recurring coronal magnetic reconnection. In this process, the estimated minimum loss in the magnetic energy is sufficient to account for the total energy required to launch the jet.

Key words. Sun: activity – Sun: corona – Sun: flares – Sun: magnetic fields – Sun: UV radiation – Sun: X-rays, gamma rays

1. Introduction

Jet-like phenomena observed in the solar atmosphere include both hot and cool plasma ejections such as X-ray jets, extreme ultraviolet (EUV) jets, and Hα surges. Shimojo et al. (1996) examined the statistical properties of 100 jets observed with *Yohkoh*/Soft X-ray Telescope (SXT), finding most jets are associated with microflares at their footpoints. The majority of X-ray jets (70%) are situated in mixed or satellite magnetic polarity regions (Shimojo et al. 1998a). Alexander & Fletcher (1999) made a comparison of jets observed in X-ray with *Yohkoh*/SXT and in EUV with the *Transition Region and Coronal Explorer (TRACE)*. They found that the physical properties and energetics of these events were in qualitative agreement with the magnetic reconnection model by Yokoyama & Shibata (1995, 1996), in which both the cool and hot (X-ray) ejected plasma is accelerated by the high pressure due to the collision of the reconnection outflow with the coronal magnetic field. Another example of a multi-wavelength jet study is given by Ko et al. (2005) who

analysed an event at the limb using *SoHO*/CDS, SoHO/EIT, *TRACE* and Mauna Loa Solar Observatory data, and at 1.64 $R_{\odot}$ using *SoHO*/UVCS observations. Chae et al. (1999) observed EUV jets and associated Hα surges that repeatedly occurred in regions of magnetic cancellation between pre-existing magnetic flux and newly emerging flux of opposite polarity.

Overall, most of the previous studies seem to support an association between microflares, X-ray jets, and cooler plasma ejections in regions of evolving magnetic field. However, the precise magnetic field evolution (flux emergence and/or cancellation) and its role in producing these dynamically-related phenomena are still not clear. In all probability, this is primarily due to the limited spatial and temporal resolution of the past observations. Recent observations taken with the *Hinode* solar satellite can help advance our understanding of the physical mechanisms responsible for the observed associated phenomena, including X-ray jets, EUV jets, and their associated microflaring activity. Chifor et al. (2008, hereafter Paper I) have reported *Hinode* observations of a recurring X-ray jet on 2007 January 15/16. The main focus of the analysis presented in Paper I was the observation of one jet instance which was observed with the EUV Imaging Spectrometer (EIS: Culhane et al. 2007)

on board *Hinode*. In Paper I we found an instance of jet plasma emission co-existing over a wide range of temperatures (Log T_e = 5.4–6.4) and having a strongly blue-shifted component (exceeding 150 km s^{-1}). The jet up-flow was found to be extremely dense (above Log N_e = 11), with a very small filling factor (<3%). It was suggested in Paper I that *multiple, small-scale* magnetic reconnection events are likely to be responsible for the production of both X-ray and EUV jets. These observations support a scenario in which jets represent the evaporation flow produced by magnetic reconnection (as proposed by Shimojo et al. 1996).

In this paper we present a further detailed analysis of the recurring jet reported in Paper I, using data from all three instruments on board *Hinode*, and complementary observations from the *Reuven Ramaty High Energy Spectroscopic Imager* (*RHESSI*: Lin et al. 2002) and the *STEREO*/Sun Earth Connection Coronal and Heliospheric Investigation (SECCHI)/Extreme Ultraviolet Imager (EUVI: Wüelser et al. 2004). One of the remaining unknowns from Paper I is the relationship between the magnetic field evolution and the production of the recurring X-ray jet. In this paper, we investigate this relationship by examining the magnetic-field data from *Hinode*/Solar Optical Telescope (SOT: Tsuneta et al. 2008). Another outstanding question in Paper I was the association between the recurring X-ray jet seen in images taken by the X-ray Telescope (XRT: Golub et al. 2007) on board *Hinode* and EUV jets, including the EUV jet instance observed by EIS and studied in Paper I. To investigate this correlation, the analysis presented in this paper includes further EUV observations from *STEREO*/SECCHI/EUVI.

This paper is organized as follows: the multi-wavelength observations and data processing are described in Sect. 2. We summarise our results in Sect. 3, while a discussion and conclusions are presented in Sect. 4.

2. Observations and data processing

2.1. Hinode/XRT and SOT observations of the recurring jet

A recurring solar X-ray jet was observed close to the NOAA active region (AR) 10 938, on its western side, associated with an X-ray bright point (XBP). We began our observations on 2007 Jan. 15 at 22:15 UT when the XBP and jet were imaged with XRT. XRT observed with a cadence of 1 min and a spatial resolution of 2″ using the "Thin Al_poly" filter which covers a temperature range of 2–10 MK. We calibrated the XRT data FITS files using the SSW *xrt_prep* routine. The XRT images contain some pointing jitter due to small spacecraft motions, as well as orbital thermal changes that slightly modify the geometry of the instrument with respect to the spacecraft. To correct for these effects, we used the jitter information in SSWDB and the SSW *xrt_jitter* routine.

The X-ray jet re-occurred at the same location (coinciding with the location of the XBP) several times between 22:16 and 02:29 UT. Figure 1 shows the lightcurves measured from XRT images around the XBP where the recurring jet occurred. The XBP gradually decreased in intensity with time (observed as a "steady" lightcurve component), then disappeared at approximately 02:30 UT. The X-ray jet bursts also became fainter with time. The first X-ray jet instance detected by XRT was associated with a microflare of *GOES* class B1.9 peaking at 22:14 UT. The second X-ray jet instance observed by XRT between 22:22–22:40 UT is shown in the image sequence in Fig. 2. Before the jet ejection, we observed an expanding "pre-jet loop"
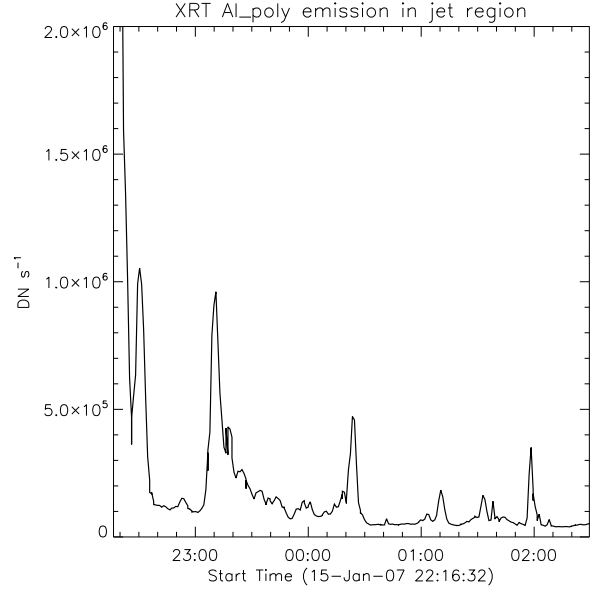

Fig. 1. X-ray emission measured from XRT images around the XBP where the recurring jet occurred (inside the red box marked in Fig. 3).

(indicated in the image taken at 22:22 UT in Fig. 2) near the footpoint of the jet. The pre-jet loop was visible until 22:33 UT, when it disconnected, just after the jet instance was released at 22:28 UT. A "post-jet" loop (bigger than the initial loop) became visible in the 22:36 UT image. Although X-ray loops were observed in the subsequent, fainter events, they became much smaller (and less evident) than the loop structures observed during the first two jet instances (at 22:18 UT and at 22:28 UT). Using XRT images of an X-ray jet in the quiet Sun, Shimojo et al. (2007) reported expanding loops "breaking" just before the jet emission occurs. They point out that their observation shows that the re-configuration of magnetic structures started before the main energy release.

We used data from the *Hinode*/SOT to determine the properties of the magnetic field regions from which the X-ray jet was launched. *Hinode*/SOT observations in our analysis were taken at two wavelengths: (1) Ca II H 3968.5 Å and (2) Fe 6302 Å Stokes *I* and *V*. The images in the first wavelength were obtained through the broad-band filter imager (BFI) and images in the second wavelength through the narrow-band filter images (NFI). In our observations, the cadence is 1 min and the spatial resolutions are 0.108″/pixel for the BFI images and 0.16″/pixel for the NFI images.

Figure 3 shows SOT/Stokes *V* and SOT/Ca II H images coaligned with the XRT data using the offsets derived by Shimizu et al. (2007). The overlays indicate that the X-ray jet was situated in a region of cancelling magnetic flux of negative polarity (plotted in white in the NFI images shown in Fig. 3). The cancelling negative flux is located at approximate coordinates (–509, 120) in the images taken at 22:16 UT (Fig. 3, top row), close to a cancelling positive flux region (plotted in black). We note that there is a small gap between the cancelling magnetic polarities. The cancelling fluxes are located south-west of a pore represented by the positive (black) polarity at the approximate coordinates (–518, 125).

Observations of the event in Ca II H (Fig. 3, Col. 2) show two ribbon brightenings associated with each X-ray jet instance: one along the south-west side of the positive pore, and the other co-aligned with the negative (white) cancelling polarity. These
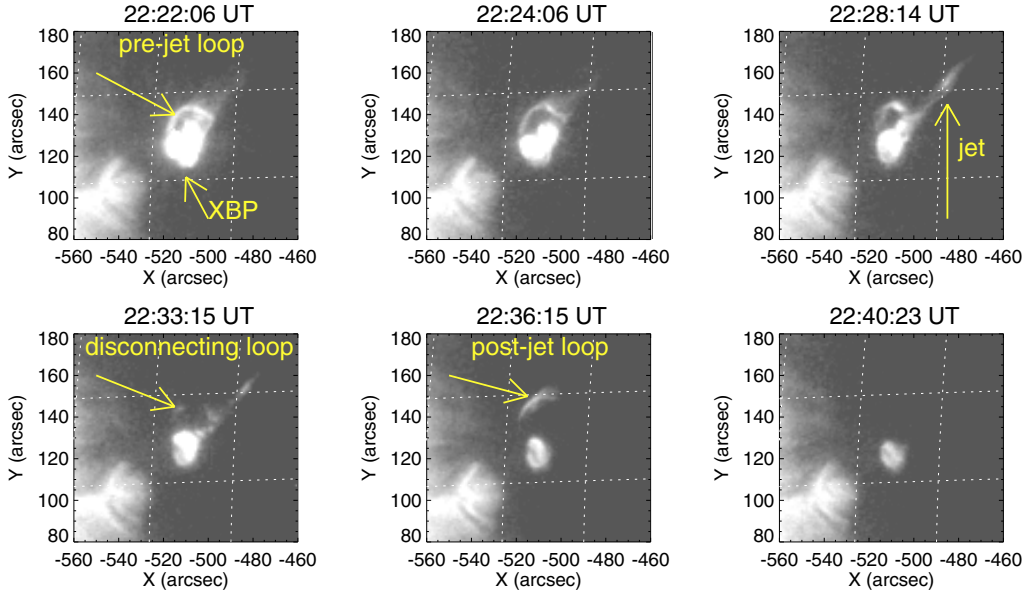
Fig. 2. The evolution of an X-ray jet instance and associated loops observed by *Hinode*/XRT ("Thin Al_poly" filter). The X-ray bright point (XBP) is indicated in the image taken at 22:22 UT.

flare-like ribbons indicate a similarity to a "standard flare" associated with magnetic cancellation. We observed the separation between the Ca II H brightenings decreasing in time. We note that this observation is consistent with the X-ray loop structures associated with the X-ray jets, which become much smaller in the jet instances after 22:28 UT. The Ca II H brightenings occurred almost simultaneously with the X-ray bursts. However, the Ca II H flux started to increase slightly earlier than the X-ray flux (this is particularly noticeable in the 00:20 UT event). In each of the first two jet instances at 22:18 UT and 22:28 UT, apart from the two ribbon brightenings, we observed a Ca II H loop expansion, followed by eruption, and a brightening northwest of the pore in the Ca II H images (indicated in Fig. 3, second row). The expanding/erupting pre-jet Ca II H loops appear to correspond to the pre-jet X-ray loops observed in simultaneous XRT images to expand and disconnect. In the subsequent jet instances, Ca II H brightenings were only clearly seen in the form of the two ribbons on the south-west side of the pore (which is consistent with the smaller and fainter XRT loops associated with later events).

2.2. Magnetic field estimation

To calibrate the SOT Stokes *IV* data we used the SSW *fg_prep* routine which subtracts the dark current from the images. We note that currently there is no flat field correction available for NFI data. From the Stokes *I* and *V* images at –120 mÅ of the Fe 6302 Å line, we calculated the line-of-sight magnetic field B in Gauss units using the empirical expressions determined by Chae et al. (2007). We applied Eqs. (7) and (8) from their paper to regions where $C_i/C_{background} > 0.4$ and $C_i/C_{background} < 0.35$, respectively, where C_i represents the counts in the Stokes *I* images and $C_{background}$ is the average intensity of the quiet Sun. For $0.35 < C_i/C_{background} < 0.4$, we applied a weighted mean, according to the same paper.

Figure 4 (left) shows the evolution of the magnetic fluxes measured from SOT/NFI images inside the area marked by the yellow box in Fig. 3. The magnetic flux evolution is compared in Fig. 4 (right) with the X-ray emission inside the jet area (marked

by the red box in Fig. 3), and with the measured Ca II H emission in the same region. The plot shows a recurring, rapid decrease in the magnetic flux (almost step-wise for the negative flux during jet instances at 23:09 UT and 00:21 UT), just before the production of an X-ray jet instance. We note that there is a small increase in the positive polarity, peaking just before 02:00 UT. However, the area in which we calculated the magnetic flux is dominated by the negative polarity conspicuous in the SOT/NFI images (we chose this area such that the decrease in negative flux by advection through the box boundary is negligible). The XBP (from which the jets were launched) had disappeared when the negative flux was completely cancelled. This strongly indicates that both the XBP heating ("steady" lightcurve component) and the recurrent jet (bursty lightcurve component) have been powered by the magnetic cancellation.

Assuming a line-of-sight scale (L) scale of 3×10^8 cm (which is roughly the diameter of the cancelling flux at the beginning of our observations), and a horizontal scale of similar order, the volume (V) where energy was dissipated is 2.15×10^{24} cm^{-3}. The decrease in magnetic energy ($E_b = B^2V/8\pi$) with each jet instance has a lower limit of 3×10^{29} erg. We estimated the cancellation rate (per unit length) to be approximately 10^7 G cm^{-1} s^{-1} during the most rapid flux cancellations observed. Shimojo et al. (1998b) estimated a thermal energy content of 10^{25}–10^{27} erg for 14 jets observed with SXT. These authors modelled the X-ray jet emission assuming a total input energy of 4×10^{28} erg. Their simulations of chromospheric evaporation based on the reconnection model reproduced the observed properties of jets well. Therefore, in the case of our observation, there would be enough magnetic energy release to explain the X-ray jet emission. We presume that a significant fraction of the energy was not dissipated and submerged, although it is difficult to conclude this from the analysed data.

From cross-comparison with SOT Spectro-Polarimeter (SP) data, Chae et al. (2007) found that a 10% relative error of the spatially integrated magnetic flux derived from their formula using SOT Stokes *IV* data. Since our data is different from those used by Chae et al. (2007), a possible difference of the filter temperature and the gradual change of filter transmission may cause
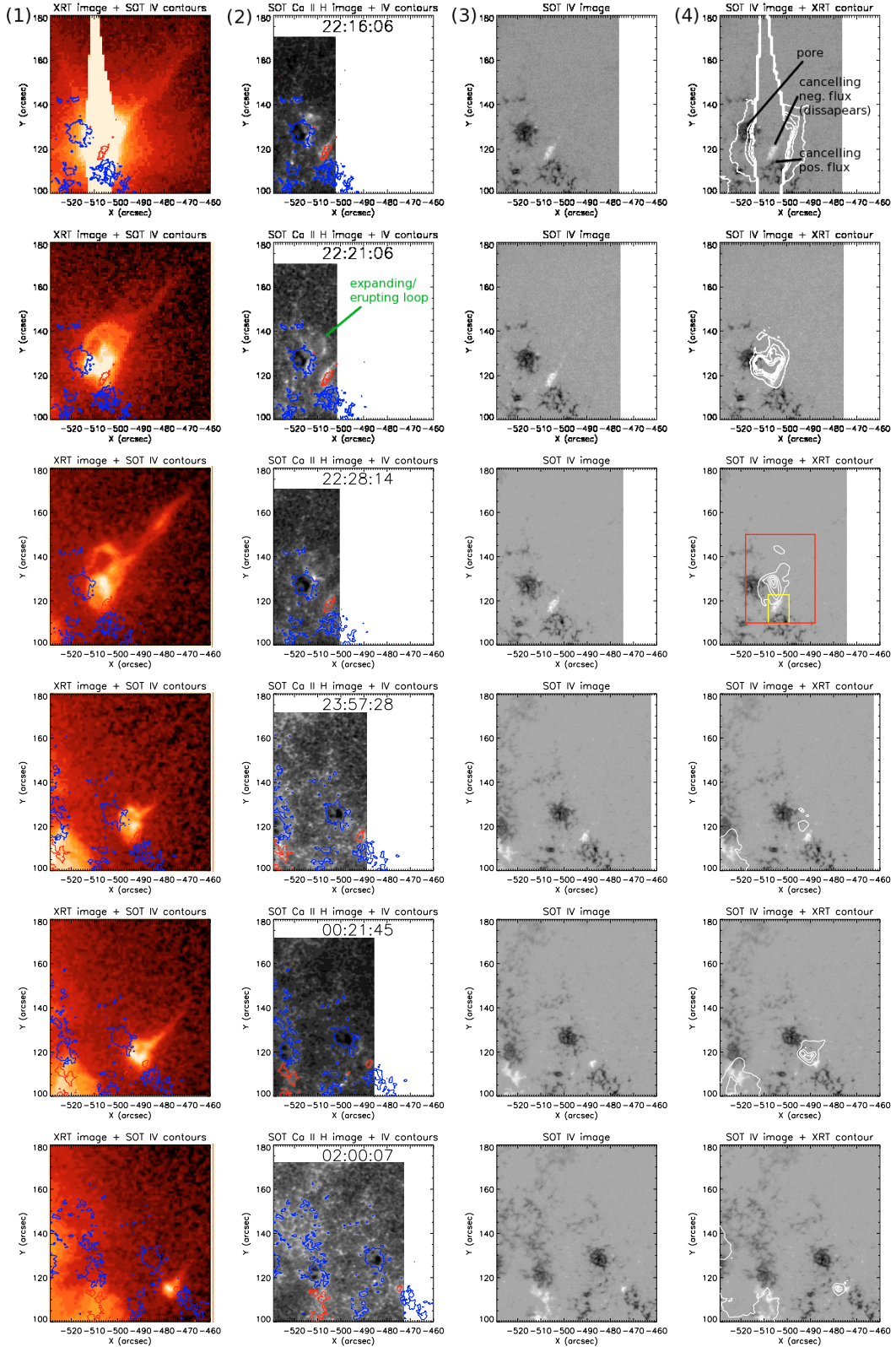
Fig. 3. (1) XRT images of several jet instances with near simultaneous SOT/FG Stokes *V* contours overplotted (positive contours plotted in blue, and negative contours in red). (2) The same SOT Stokes *V* contours overlaid on co-temporal Ca II H images. (3) The SOT/FG Stokes *V* magnetogram images. (4) SOT/FG Stokes *V* magnetogram images with XRT contours superimposed (positive polarity plotted in black and negative polarity in white). The cancelling magnetic region with the positive flux eventually disappearing is located at the approximate coordinates (−509, 120) in *the top panels* taken at 22:16 UT (times given correspond to the XRT images). The positive pore is located at approximately (−518, 125). We performed the co-alignments using the offsets provided by Shimizu et al. (2007). The yellow box on the right panel at 22:28:14 UT (*bottom row*) marks the cancelling magnetic region in which we measured the magnetic fluxes. The red box marks the region in which we measured the X-ray and Ca II H emissions.
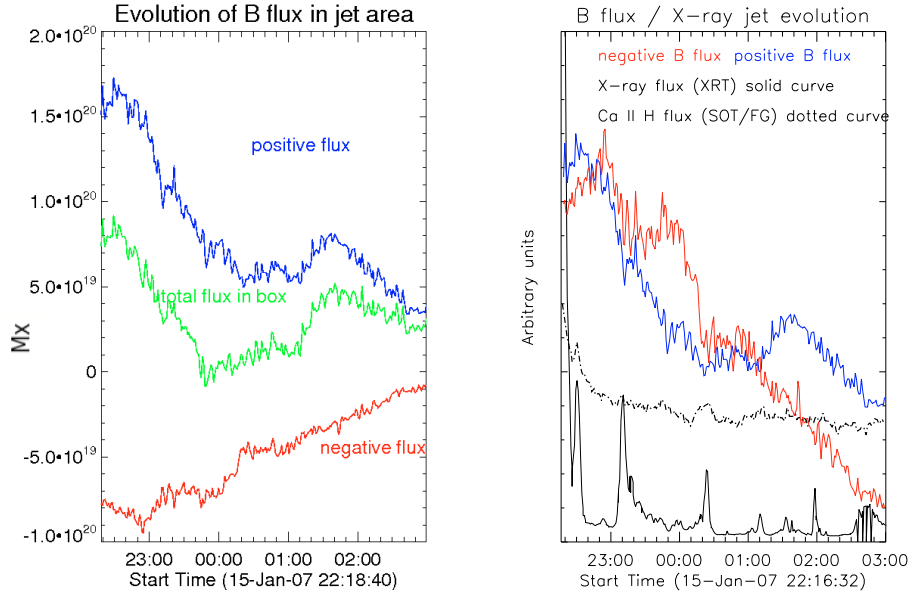
Fig. 4. *Left*: measured magnetic fluxes (in Mx units) from the calibrated SOT/NFI data inside the region of the observed cancelling negative polarity (yellow box marked in Fig. 3, third row). *Right*: comparison between the recurring X-ray jet emission (black, solid curve) measured from XRT images inside the red box marked in Fig. 3 (same lightcurves shown in Fig. 1), the SOT Ca II H emission in the same region (black, dotted curve), and the magnetic fluxes measured from SOT/NFI images inside the yellow box marked in Fig. 3. The plot indicates a recurring cancellation of the magnetic fluxes, with recurring, abrupt decreases in the positive and negative fluxes just before the ejection of each jet. This decrease is particularly abrupt during the jet instances at 23:09 UT and 00:21 UT. The *y* axis units are arbitrary.

a further error in the absolute value of our measured magnetic fluxes. However, the relative change in the magnetic flux should be more accurate than the absolute value, and therefore the observed abrupt decrease of the magnetic fluxes is a robust feature.

2.3. Associated microflaring emission observed with RHESSI

The first X-ray jet detected by XRT was associated with a microflare of *GOES* class B1.9 (Fig. 5) peaking at 22:14 UT in both the *GOES* and *RHESSI* lightcurves. Simultaneous with the microflare emission, the radiospectrograph of the Culgoora Solar Observatory detected a type III radio burst (Fig. 5). The same instrument detected two subsequent smaller type III radio bursts at 22:28:40 UT and 22:29:53 UT. These radio bursts correspond to one instance of the X-ray jet seen in XRT images.

RHESSI images were obtained for the X-ray emission in 4–8 keV and 12–16 keV during 22:13:40 UT to 22:14:40 UT and were overlaid on the softer XRT images (Fig. 6). The closest XRT image in time to the *RHESSI* images occurred at 22:16 UT, during which the bright microflare emission has saturated the XRT image. This rendered the co-alignment of the images difficult, though the *RHESSI* contours lie within the saturated XRT spike implying they are close. Therefore no co-alignment has been attempted. The emission observed with *RHESSI* is close to the subsequent footpoints of the later cusp-shaped jet visible in the 22:19 UT XRT image, suggesting that it is likely to be spatially coinciding with the cancelling negative polarity observed in the SOT Stokes *V* images.

The *RHESSI* spectrum of the microflare during 22:13:40 UT to 22:14:40 UT was fitted with a combined thermal and nonthermal bremsstrahlung spectrum (as shown in Fig. 6). A temperature of 13 MK was found, which is slightly higher than typical for *RHESSI* microflares (Hannah et al. 2008). The
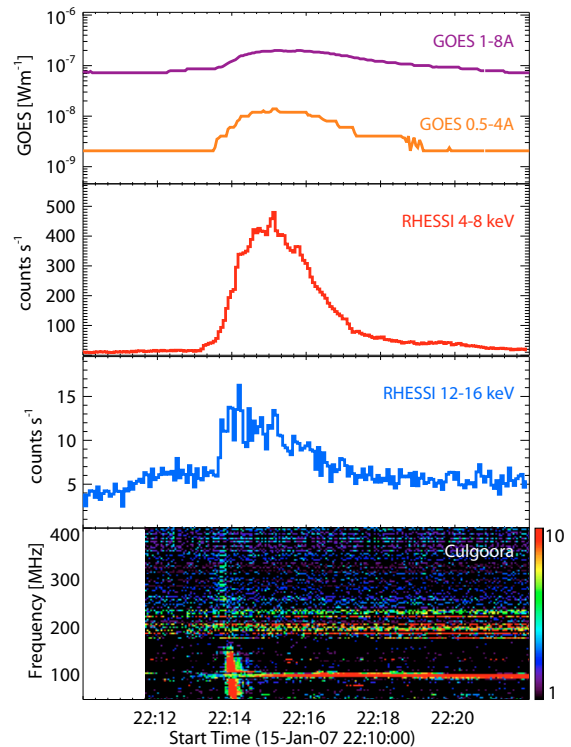

Fig. 5. *GOES* 1–8 and 0.5–4 Å (*top panel*) and *RHESSI* 4–8 and 12–16 keV lightcurves showing that a microflare occurred at the time of the first observed X-ray jet instance in *Hinode*/XRT images. Culgoora radiospectrograph detected a type III radio burst (*bottom panel*) at the time of the microflare associated with the jet instance.

non-thermal emission has been fitted with a broken power law, with a fixed index of –1.7 below the break, approximating the estimated flattening of the non-thermal emission in this energy
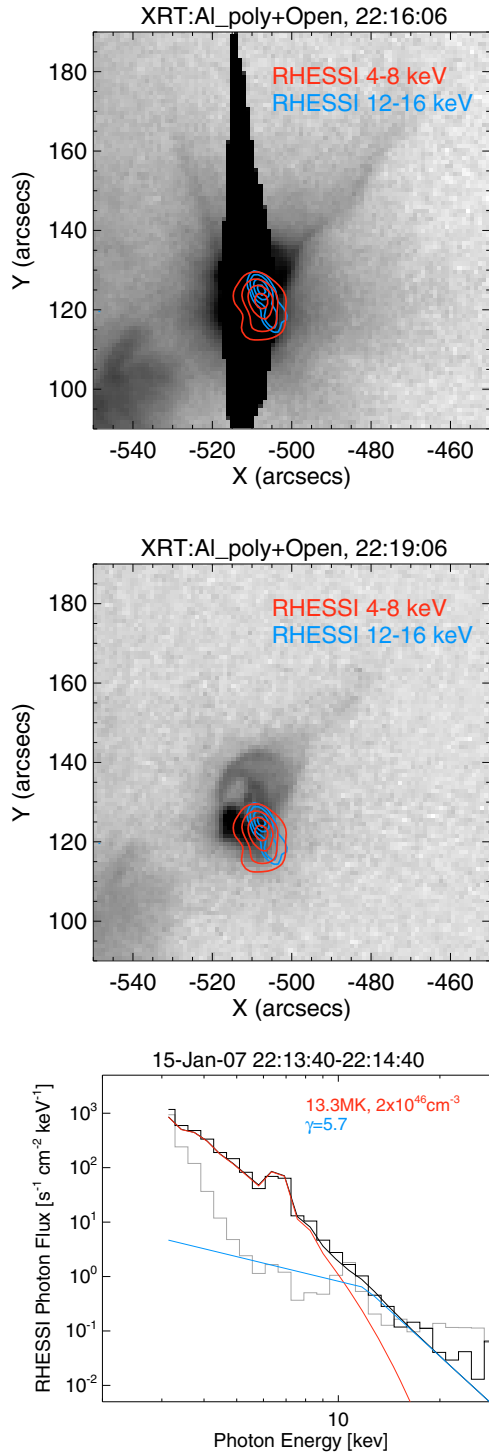
Fig. 7. Comparison of an X-ray jet observed with *Hinode*/XRT (*right panels*) and a simultaneous EUV jet observed by *STEREO*/SECCHI/EUVI in its 195 Å filter (*left panels*). *The bottom panels* show the XRT contours overlaid on the XRT image (*left*) and on the EUVI image (*right*).

Fig. 6. *Top*: *RHESSI* high-energy emission contours imaged during the the most impulsive part of the jet-associated microflare (between 22:13–22:15 UT) are overlaid on the XRT image taken at 22:16 UT (the XRT image is saturated). The accuracy of the co-alignment is estimated to be better than 5″. The *RHESSI* 4–8 keV emission is plotted in red, and the 12–16 keV emission is plotted in blue. Middle: same *RHESSI* contour as in *the top panel*, plotted on an XRT image taken at 22:19 UT. *RHESSI* high energy emission matches the footpoint of the cusp-shape soft X-ray jet. *Bottom*: fitted *RHESSI* photon spectrum accumulated in detector 1. The subtracted background emission is plotted in grey. The thermal microflare emission is fitted with a thermal bremmstrahlung function (plotted in red). A standard thick-target model was included in the fit (plotted in blue).
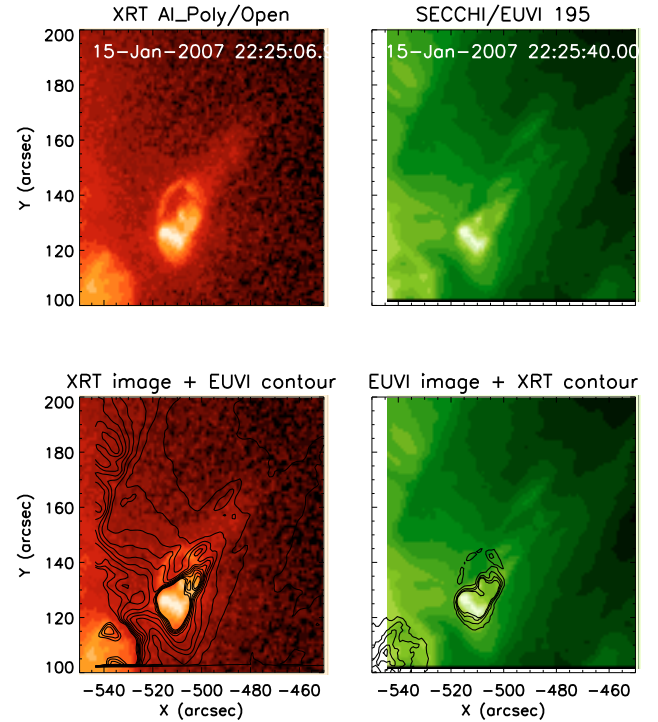
range (Holman 2003). Since only little of the spectrum is greater than 3 sigma at energies above 12 keV, one cannot reliably estimate the non-thermal energy. This slightly higher temperature and the difficulty in determining the higher energy emission from background is likely due to the degraded performance of *RHESSI*'s detectors from radiation damage. Nevertheless, the type III radio burst associated with the microflare represents supporting evidence for the non-thermal emission associated with the event.

2.4. Associated EUV jets observed with STEREO/SECCHI/EUVI

Simultaneous with the recurring X-ray jet, we observed a series of EUV jet instances in full-disk images taken by the SECCHI/EUVI instrument on board *STEREO* (A). EUVI observed the jet instances through its 171 and 195 Å filters with a cadence of 10 min and a pixel size of 1.59″. The EUV jet instances are co-spatial with the X-ray jet observed in the XRT images (Fig. 7). We co-aligned the *STEREO*/SECCHI/EUVI and XRT data using simultaneous SECCHI/EUVI 284 Å filter images and XRT "Thin Al_poly"/Open images. Figure 7 shows the co-alignment between an XRT image taken at 22:25 UT and a simultaneous EUVI 195 Å image. The EUV jet had a similar direction and collimated shape as the X-ray jet, but we identified slight differences in morphology, with the jet-associated loops visible only in the XRT images, suggesting that the loops are hotter than the jet emission.
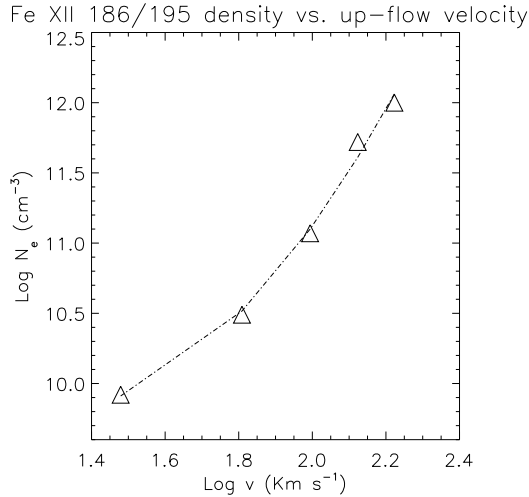
Fe XII 186/195 density vs. up−flow velocity

Fig. 8. Density values calculated from the Fe XII ($\lambda186/\lambda195$) profile ratio in the blue-shifted wings of the lines observed in the up-flow component (same data as Fig. 4 of Paper I, but plotted in the log here). The power fitting law yields $N_e \propto v^{2.55}$.

2.5. An instance of the associated EUV jet observed by Hinode/EIS

Starting with 00:54 UT on Jan. 16, EIS ran an observing study called "HH_AR+FLR_RAS_N01(J)" three times over AR 10938. We analysed the data taken by the first raster from this sequence (between 01:54:11–02:20:27 UT), with EIS rastering over the location the jet images at ~02:01 UT. A detailed analysis of this observation which led to the measurement of flows, density and filling factor were given in Paper I, and therefore, is not repeated in the present paper. In Paper I we found an extremely dense (above Log N_e = 11), and strongly blue-shifted jet component (exceeding 150 km s^{-1}), the density being proportional to the up-flow velocity (Fig. 8).

3. Summary of results

We summarize the results of the analysis given in this paper as following:

1. The recurring X-ray jet was associated with an XBP located in a region of cancelling magnetic flux, close to a pore.
2. We found a correlation between a recurring magnetic flux cancellation, the emission of the X-ray jet and associated brightenings in Ca II H images. The recurring X-ray and Ca II H jet emission decreased in intensity with each jet instance.
3. Ca II H ribbon brightenings were observed in association with each X-ray jet instance: one along the south-west side of the positive pore, and the other co-aligned with the negative cancelling polarity. Ca II H brightenings occurred almost simultaneously with the X-ray bursts, but the Ca II H flux started to increase slightly earlier than the X-ray flux.
4. The decrease in magnetic energy with each jet instance has a lower limit of approximately 3×10^{29} erg. The magnetic cancellation rate (per unit length) was estimated at ~10^7 G cm^{-1} s^{-1}, during the most rapid magnetic flux decreases.
5. The associated XBP disappeared almost at the same time as the eventual disappearance of the cancelling polarities.

6. "Pre-jet" X-ray loops were observed to expand near the foot-point of X-ray jet instances, disconnecting just after an X-ray jet instance is released, followed by the appearance of "post-jet" loops (bigger than the "pre-jet" loops). Associated with the X-ray loops, we found Ca II H "pre-jet" loops expanding and erupting.
7. The recurring plasma ejection was observed simultaneously at EUV and X-ray temperatures. The EUV jet had the same location, direction and collimated shape as the X-ray jet, but we identified slight differences in morphology, with the jet-associated loops visible only in the XRT images.
8. Type III radio bursts were detected simultaneously with the first two X-ray jet instances observed.
9. A hot microflare ($T \sim 13$ MK) was observed by *RHESSI* at the footpoint of the first X-ray jet instance. The location of the hard X-ray source is close to the side of the soft X-ray microflare, corresponding to the magnetic cancellation site.

4. Interpretation and discussion

In this paper we analysed, for the first time, a recurring solar jet observed in X-ray and EUV with all three instruments of the *Hinode* observatory, together with complementary observations from *RHESSI* and *STEREO*/SECCHI/EUVI. This paper furthers the preliminary analysis reported in Paper I to study the role of magnetic cancellation in the production of recurring solar EUV and X-ray jets.

4.1. Location of magnetic reconnection

It is widely accepted that magnetic reconnection is the most plausible explanation for magnetic cancellation in the photosphere. (Note, however, that there is evidence for cancellation by U-loop emergence by van Driel-Gesztelyi et al. 2000). However, the exact location of the reconnection point has not been established. Some authors considered that the temperature minimum region (upper photosphere) is favorable to reconnection because the resistivity is largest there (Priest et al. 1994; Litvinenko et al. 1999). Bellot Rubio & Beck (2005) analysed cancellation events in the moat region of a sunspot. They found no significant changes in field strength, field inclination or temperature associated with cancellation and concluded that the reconnection took place in the photosphere.

On the other hand, transition region and coronal brightenings have also been observed associated with photospheric cancellation, suggesting the transition region or the corona for the location of reconnection (Dere et al. 1991; Chae et al. 1998; Madjarska et al. 2001). In this case, the reconnection loop must submerge below the photosphere to be observed as a cancellation. Evidence for submergence has been reported by Harvey et al. (1999) and Chae et al. (2004). Most likely the height of reconnection and its observational consequences are different for different events, depending on the size, structure and interaction with the surrounding environment (such as convection) of the cancelling magnetic flux (Parnell et al. 1994; Isobe et al. 2007; von Rekowski & Hood 2008).

Although it is difficult to reliably identify a nonthermal component in the *RHESSI* microflare spectrum for the jets studied here, the type III radio burst strongly supports the existence of a nonthermal electron beam. This microflare observation is strongly suggestive of magnetic reconnection taking place in the corona. This is because such high temperature plasma and non-thermal electron beam are unlikely to be produced in the dense chromospheric plasma. Hard X-ray emission was not observed
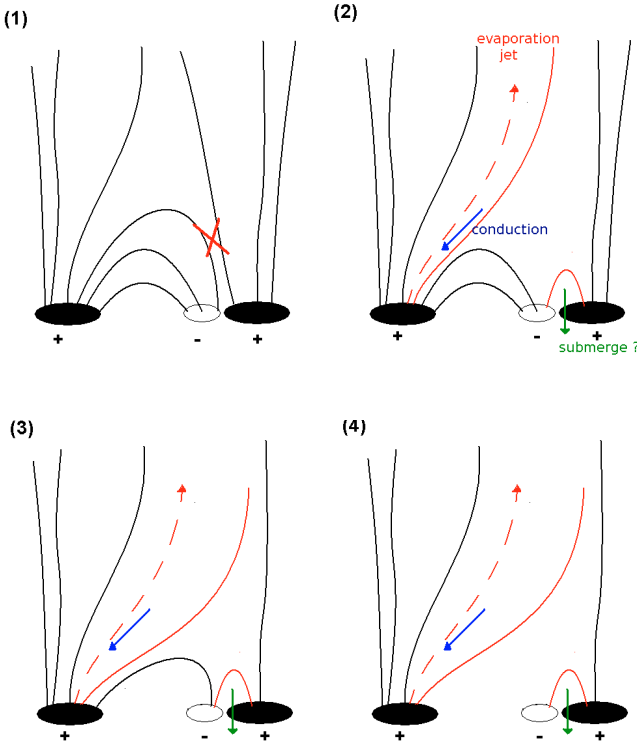
(1) **(2)**

(3) **(4)**

Fig. 9. Cartoon representing our interpretation of the magnetic field configuration and evolution during three instances of a multi-thermal jet produced by magnetic cancellation. The continuous lines represent the magnetic field lines, with the left positive polarity representing the pore, and the smaller, negative polarity representing the cancelling (and eventually disappearing) negative flux. The right positive polarity repeatedly cancels with the small negative polarity. The red lines indicate magnetic field lines which have just reconnected. The observed Ca II H ribbon brightenings are located at the footpoints of the just-reconnected magnetic field lines while the high energy X-ray source is located above the cancellation site.

by *RHESSI* in the later events, but two subsequent type III bursts were detected. This may be due to a smaller energy release in a smaller volume. The location of the hard X-ray source as seen by *RHESSI* is close to the side of the soft X-ray microflare, corresponding to the magnetic cancellation site. This is evidence that reconnection is taking place just above the cancellation site. The "gap" between the cancelling polarities observed in the SOT NFI data represents further supporting evidence for coronal magnetic reconnection.

On the other hand, the Ca II H emission peaks precede the soft X-ray peaks. This may suggest that the first energy release (i.e., by reconnection) occurred in the chromosphere and then the energy is transferred to the corona where X-rays are produced, contrary to the interpretation given above. However, this is in fact consistent with the evaporation scenario. In the evaporation scenario, the released energy in the corona is transported to the chromosphere. Coronal X-ray emission in this stage is weak because of the small coronal density. The heated chromospheric plasma ablates, supplying hot and dense plasma in the corona. The coronal X-ray emission drastically increases at this stage. Therefore it is natural that chromosphere brightens first and the corona next.

4.2. Role of recurring magnetic reconnection in the corona for jet production

The cartoon shown in Fig. 9 represents our interpretation of the multi-wavelength observations. The magnetic field configuration prior to reconnection is sketched in the first panel (1) of Fig. 9, the left positive polarity representing the pore, and the smaller, negative polarity representing the cancelling (and eventually disappearing) negative flux. The right positive polarity repeatedly cancels with the small negative polarity (panels 2–4 of Fig. 9). The field lines which have just reconnected are plotted in red, and the observed Ca II H brightenings are located at the footpoints of these lines. We note that, according to this interpretation, there should be three Ca II H ribbon brightenings, as observed in the first jet instance at 22:18 UT. However, because the cancelling polarities are very close to the FOV edge of the Ca II H images, it is likely that the Ca II H brightening corresponding to the right (cancelling) positive polarity is located outside the FOV, and therefore not observed. Sakajiri et al. (2004) reported an observation of converging flare ribbons in a microflare associated with emerging flux. In our event, the separation of Ca II H brightenings becomes smaller in later events. It is possible that the magnetic configuration that causes such converging behaviour is the same for both events. The loop-like ejections associated with the jet observed in Ca II H and X-ray may correspond to a plasmoid or flux rope formed by tearing instability in the reconnecting current sheet (Priest et al. 1994; Yokoyama & Shibata 1996).

In Paper I we pointed out that the high density, coupled with small filling factor, and large velocities represent strong evidence of multiple, small-scale magnetic reconnection occurring in a small region being responsible for the production of (EUV and X-ray) jets. In this paper, we found a correlation between the recurring magnetic field cancellation and the production of recurring EUV and X-ray emission in this paper, which supports the conclusion drawn in Paper I. In this process, the estimated minimum loss in the magnetic energy (3×10^{29} erg) is sufficient to account for the total energy required to launch the jet. We estimated the magnetic cancellation rate (per unit length) to be of the order of 10^7 G cm^{-1} s^{-1} when the rapidly cancelling flux is associated with jet production.

4.3. Evaporation scenario

In Paper I we reported a correlation between the velocity and density of the jet observed by EIS, and concluded that it is evidence for an evaporation jet, i.e., driven by the gas pressure gradient. Here we present more detail discussion.

First, we re-visit the discussion by Shimojo et al. (2001) in which they derive the relationship between density (n_{eva}) and velocity (v_{eva}) of the evaporation jet. For convenience, we use the same notation as used by Shimojo et al. (2001). The maximum jet velocity is approximately given by the sound velocity, C_s, (Fisher et al. 1984):

$$v_{eva} \sim C_s \propto \sqrt{T}. \tag{1}$$

(Eq. (15) of Shimojo et al. 2001) When the radiative cooling is neglected, the conductive heat flux from the corona balances the enthalpy flux of the jet:

$$\frac{\kappa_0 T^{7/2}}{s_{flare}} \sim \frac{\gamma}{\gamma - 1} P v_{eva} \tag{2}$$

(Eq. (16) of Shimojo et al. 2001). s_{flare} represents the height of energy deposition, which corresponds to the height of reconnection, and P is the pressure of the evaporating plasma.

Using this equation, and $P = 2n_{eva}k_b$ T, the mass flux of the jet can be written as:

$$m_p n_{eva} v_{eva} \sim \frac{\gamma - 1}{\gamma} \frac{m_p \kappa_0 T^{5/2}}{2 k_B s_{flare}} \quad (3)$$

where m_p is the mass of the proton. Hence, using Eq. (15) of Shimojo et al. (2001) and assuming s_{flare} is constant,

$$n_{eva} \propto \frac{T^{5/2}}{v_{eva}} \propto T^2 \propto v_{eva}^4. \quad (4)$$

Figure 8 shows the correlation of velocity and density observed by EIS (same data as Fig. 4 of Paper I, but plotted in the log). The power law fitting yields $n_e \propto v^{2.55}$. The exponent is smaller than the theoretical prediction. However, the theoretical density and velocity of the jet are at their maximum, while those derived from observations would be an average weighted with the emission measure. Taking this into account, we conclude that the evaporation theory is in good agreement with our observations.

Note that if we considered an evaporation flow along *one* flux tube, one would expect an anti-correlation of velocity and density because mass flux $n_{eva} v_{eva}$ would be constant along the flux tube. However, the small filling factor we measured in Paper I (at most 3%) suggests that the jet consists of many thin, unresolved jets, which may have been caused by multiple small-scale magnetic reconnection in the corona. In this case, it is important to note that each unresolved elemental flux tube (jet) would have a different energy deposition. Since both density and velocity are positively correlated with the deposited energy, our observations support the evaporation scenario in jets, being consistent with the simulations ran by Shimojo et al. (2001).

4.4. Jets and associated activity (microflare, radio bursts) observed at multi-wavelength

We observed the recurring plasma ejection simultaneously at both EUV and X-ray temperatures. The EUV jet had the same location, direction and collimated shape as the X-ray jet, but we identified slight differences in morphology, with the jet-associated loops visible only in the XRT images, suggesting that the loops are hotter than the jet emission. Previous studies by Alexander & Fletcher (1999) found differences in the morphology between the EUV and X-ray jets, with the EUV jets having an apparent twisting motion. These rotations were also confirmed by Jiang et al. (2007) who reported EUV jets associated with soft X-ray jets and Hα surges, pointing out the possible role of flux cancellations in generating the observed phenomena. Although we did not observe a rotation for the EUV jet in the SECCHI/EUVI images, our observations were limited by the 10 min cadence at which they were obtained.

Based on high-cadence *TRACE* EUV and XRT X-ray observations of jets, Kim et al. (2007) suggest the possibility of a multi-thermal structure in jets, as previously suggested by Yokoyama & Shibata (1996). However, the same authors mention that their observations were limited by the fact that only one single XRT filter was used, and they could not estimate the temperatures of the jets. In Paper I we presented an analysis of EIS observations for one instance of the recurring jet presented in this paper (being well correlated with the XRT and SECCHI/EUVI jet instances). These observations have shown

that the jet up-flow co-existed over a wide range of temperatures (Log T_e = 5.4–6.4), confirming the multi-thermal nature of jets.

Ko et al. (2005) found an electron temperature of 1.6×10^5 K and density of 10^7 cm^{-3} for their jet observed in the O VI line emission at an altitude of 1.6 $R_\odot$ with *SoHO*/UVCS. The lower density found by these authors using O VI diagnostics is probably due to an adiabatic expansion, as the altitude of their jet is higher. If the ejected material is rarefied from 10^{10} cm^{-3} at the base of the corona to 10^7 cm^{-3} at 1.6 $R_\odot$, then the temperature ratio is 10^{-2}. If we assume the temperature at the coronal base to be several million degree (typical for coronal jets, and consistent with the 171 Å emission found by Ko et al. (2005) at the early jet stage), then the jet could be observed at the O VI temperature. There could also be additional cooling by radiation or heat conduction. Similar to our analysis, Ko et al. (2005) also found large line broadening (2.5 above that of the background corona).

We found associated microflare emission observed with *RHESSI* at the footpoint of an X-ray jet instance, co-aligned with the cancelling magnetic flux. We note that microflares could have occurred during later (fainter) jet instances, but were likely too small to be detected by *RHESSI*. Kundu et al. (1995) have previously reported the positions of the type III bursts aligned in the direction of the X-ray jets. In our study, we found one burst associated with the first observed jet instance (associated with the *RHESSI* microflare), followed by two subsequent bursts corresponding to another X-ray jet instance. The type III radio bursts associated with both microflares and X-ray jet strongly suggest a similar origin for these phenomena. Our multi-wavelength observations have revealed the multi-thermality of the jet and the details of the associated phenomena. Complementary observations at multi-wavelength have provided strong evidence that the recurring jet and associated phenomena can be attributed to recurring magnetic reconnection taking place in the corona.

References

Alexander, D., & Fletcher, L. 1999, Sol. Phys., 190, 167
Bellot Rubio, L. R., & Beck, C. 2005, ApJ, 626, L125
Brekke, P. 1999, Sol. Phys., 190, 379
Chae, J., Wang, H., Lee, C.-Y., Goode, P. R., & Schuehle, U. 1998, ApJ, 497, L109
Chae, J., Qiu, J., Wang, H., & Goode, P. R. 1999, ApJ, 513, L75
Chae, J., Moon, Y.-J., & Pevtsov, A. A. 2004, ApJ, 602, L65
Chae, J., Moon, J.-Y., Park, Y.-D., et al. 2007, PASJ, 59, 619
Chifor, C., Young, P. R., Isobe, H., et al. 2008, A&A, 481, L57
Culhane, J. L., Harra, L. K., James, A. M., et al. 2007, Sol. Phys., 243, 19
Dere, K. P., Bartoe, J.-D. F., Brueckner, G. E., Ewing, J., & Lund, P. 1991, JGR, 96, 9399
Dere, K. P., Landi, E., Mason, H. E., Monsignori Fossi, B. C., & Young, P. R. 1997, A&AS, 125, 149
Fisher, G. H., Canfield, R. C., & McClymont, A. N. 1984, ApJ, 281, L79
Golub, L., Austin, G., Bookbinder, J., et al. 2007, Sol. Phys., 243, 63
Handy, B. N., Acton, L. W., Kankelborg, C. C., et al. 1999, Sol. Phys., 187, 229
Hannah, I., Hurford, G. J., Hudson, H. S., Lin, R. P., & van Bibber, K. 2007, ApJ, 659, L77
Hannah, I., Christe, S., Krucker, S., et al. 2008, ApJ, 677, 704
Harvey, K. L., Jones, H. P., Schrijver, C. J., & Penn, M. J. 1999, Sol. Phys., 190, 35
Holman, G. D. 2003, ApJ, 586, 606

Ichimoto, K, Suematsu, Y., Shimizu, T., et al. 2007, ASPC, 369, 39
Isobe, H., Tripathi, D., & Archontis, V. 2007, ApJ, 657, L53
Ko, Y.-K., Raymond, J. C., Gibson, S. E., et al. 2005, ApJ, 623, 519
Jiang, Y. C., Chen, H. D., Li, K. J., She, Y. D., & Yang, L. H. 2007, A&A, 469, 331
Kamio, S., Hara, H., Watanabe, T., et al. 2007, PASJ, 59, 757
Kim, Y.-H., Moon, Y.-J., Park, Y.-D., et al. 2007, PASJ, 59, 763
Kosugi, T., Matsuzaki, K., Sakao, T., et al. 2007, Sol. Phys., 243, 3
Kundu, M. R., Raulin, J. P., Nitta, N., et al. 1995, ApJ, 447, L135
Landi, E., Del Zanna, G., Young, P. R., et al. 2006, ApJS, 162, 261
Lin, R. P., Dennis, B. R., Hurford, G. J., et al. 2002, Sol. Phys., 210, 3
Litvinenko, Y. E. 1999, ApJ, 515, 435
Madjarska, M. S., Doyle, J. G., Teriaca, L., & Banerjee, D. 2003, A&A, 398, 775
Parnell, C. E., Priest, E. R., & Titov, V. S. 1994, Sol. Phys., 153, 217

Priest, E. R., Parnell, C. E., & Martin, S. F. 1994, ApJ, 427, 459
Sakajiri, T., Brooks, D. H., Yamamoto, T., et al. 2004, ApJ, 616, 578
Shimizu, T., Katsukawa, Y., Matsuzaki, et al. 2007, PASJ, 59, 845
Shimojo, M., Hashimoto, Shibata, K., et al. 1996, PASJ, 48, 123
Shimojo, M., Shibata, K., & Harvey, K. L. 1998, Sol. Phys., 178, 379
Shimojo, M., Shibata, K., Hori, K., &, Yokoyama, T. 1998, ESA-SP, 421, 163
Shimojo, M., Shibata, K., Yokoyama, T., & Hori, K. 2001, ApJ, 550, 1051
Shimojo, M., Narukage, N., Kano, R., et al. 2007, PASJ, 59, 745
Tsuneta, S., Acton, L., Bruner, M., et al. 1991, Sol. Phys., 136, 37
Tsuneta, S., Ichimoto, K., Katsukawa, Y., et al. 2008, Sol. Phys., 249, 167
van Driel-Gesztelyi, L., Malherbe J.-M., & Démoulin, P. 2000, A&A, 364, 845
von Rekowski, B., & Hood, A. W. 2008, MNRAS, 385, 1792
Yokoyama, T., & Shibata, K. 1995, Nature, 375, 42
Yokoyama, T., & Shibata, K. 1996, PASJ, 48, 353
Wüelser, J.-P., Lemen, J. R., Tarbell, T. D., et al. 2004, SPIE, 5171, 111